Orbital
The electronic journal of chemistry

the electronic journal of chemistry

Full Paper | http://dx.doi.org/10.17807/orbital.v15i1.16470

Spectral Voltage Contour Plots of Optical Constants and Interface Parameters of the Active Layer of a Multilayer Structure Suspended Particle Device Smart Window from Clear on to Dark off States

David Barrios* [a,b] and Carlos Alvarez [b]

Smart windows based on suspended particle devices (SPDs) are able to switch optically from dark to clear visual appearance when applying an AC electrical signal. This effect is due to light absorbing nanoparticles that get aligned by the applied voltage. The sandwich structure of an SPD consists of several layers and includes two outer glass substrates, each one covered on its inwards-facing side with a transparent conducting thin layer surrounding the centrally positioned SPD active layer. A knowledge of the optical constants of each layer—i.e., the complex refractive index, including its real and imaginary (absorption) parts—is a key in the design of the visual appearance of the SPD window and is a useful tool to determine the optimum thickness of the active layer.

Graphical abstract

Keywords

Optical constants
Multilayer smart windows
Suspended particle devices

Article history

Received 05 Aug 2022
Revised 23 Aug 2022
Accepted 15 Feb 2023
Available online 05 Apr 2023

Handling Editor: Grégoire Demets

1. Introduction

Chromogenic materials are able to change the transmitted, reflected, scattered or absorbed light by means of an external stimulus such as an electrical signal. Electrochromic devices (ECDs), polymer dispersed liquid crystals (PDLCs) and suspended particle devices (SPDs) are three technologies for electrically controllable transmittance of smart windows. Among the advantages of SPDs are their short switching times, of the order of a second for large area devices, and the visual appearance of the SPD's optical states, which switch from dark bluish-grey to clear grey, rather than from white-milky translucent to transparent states as in PDLCs. The major drawbacks for SPD smart windows are their relatively low transmittance in the clear state, in the range of 50%, their haze or undesired light scattering, which ensues from the absorbing and scattering particles, and the requirement of electrical power in the clear state. Currently, one of the best SPD applications is in the automotive market.

In previous works [1,2], an electro-optical characterization of an SPD sample was carried out by considering only one

[a] Grupo de Displays y Aplicaciones Fotónicas, Dept. Tecnología Electrónica, Universidad Carlos III de Madrid, C/Butarque, 15, E28911, Leganés, Madrid, Spain. [b] Universidad Politécnica Salesiana, Guayaquil, Ecuador. *Corresponding author. E-mail: dbarriosp76@gmail.com

layer for their sandwich structure (due to the unknown optical constants of the other layers). The refractive index and the extinction coefficients were determined by using the collimated-collimated (cc) equations of the Maheu-Letoulozan-Gouesbet four-flux model (MLG-4FM, [3]) for direct transmittance (T_{dir}) and specular reflectance (R_{spec}). The extensive scattering and absorption coefficients (S & K) were approximated by using the Kubelka-Munk two-flux model (KM-2FM, [4]) combined with the Saunderson corrections [5], for taking into account the interfaces, for the total transmittance and reflectance (T_{tot} & R_{tot}). In the present work, two glass substrates and two ITO (Indium Tin Oxide) thin films are added to the model of the sandwich structure surrounding the active layer containing the suspended particles, and its optical constants—i.e., refractive index and extinction coefficient—were determined by using Pfrommer's matrix model [6].

2. Material and Methods

In this section for materials and methods, the devices, optical measurements and a theory section will be detailed.

2.1 Devices

An SPD sample with 28 x 22 cm^2 active area and 1 cm total thickness was supplied by CRICURSA (Cristales Curvados S.A., Barcelona, Spain), which is a licensee of Research Frontiers Inc. (Woodbury, NY, USA). The inner active layer consists of a cross-linked polymer matrix containing droplets comprising a suspension of polyhalide particles [1]. The SPD sample operated with 0 (dark off state) and 100 V_{peak} (clear on state) and 50 Hz of frequency sinusoidal signals.

2.2 Optical measurements

A Perkin Elmer Lambda 900 spectrophotometer, equipped with an integrating sphere, was used for measuring the total and diffuse transmittance and reflectance (τ & ρ) of the SPD sample in the solar wavelength range (250 to 2500 nm) in steps of 5 nm for the dark off and clear on states. Intermediate levels of transmittance τ were also measured with 10 V steps from 0 to 100 V_{peak}.

2.3 Theory

Pfrommer method describes the matrices for interface and layers, which can be classified in substrate (or thick layers) and films (or thin layers), according to their thickness and the wavelength of incident light. This section will be divided into the following sections:

(2.3.1) Interface & layer matrices for thick layers (substrates) and thin layers (films).

(2.3.2) Transmittance and reflectance (τ & ρ) of a thick layer or substrate.

(2.3.3) Transmission and reflection (t & r) coefficients of a thin layer or film deposited over a thick layer or substrate.

2.3.1 Interface & layer matrices for thick layers (substrates) and thin layers (films)

Following the Pfrommer nomenclature [6] for the multilayer sandwich structure method, two different types of matrices are observed:

- Interface M matrices: represents the relationship between the amplitudes or intensities of the radiation fields on each side of the interface between two layers.
- Layer N matrices: describes the attenuation of the radiation as it propagates through a layer.

The transmission of radiation through an absorbing material depends on the thickness or optical path of the layers:

- A thick layer or substrate shows disturbances along the path of propagation due to in-homogeneities in the material, which disrupt the phases of the waves and destroy the coherence of the waves, resulting in a reduction of the intensity (I) of the transported energy, referred as extinction and caused by scattering and absorption.
- A thin layer thickness is of the order or the wavelength of incident light or less. The short path-differences between the waves inter-reflected between the interfaces result in interferences, which mean that the coherence of the wave is maintained. A thin layer shows absorption of light due to destructive interference, which result into an attenuation of the electric field (E).

2.3.2 Transmittance and reflectance (τ & ρ) of a thick layer or substrate

The transmission radiation through an absorption and/or scattering media is characterized by the complex refractive index n' of the material:

$$n' = n - i\kappa \qquad \text{(Eq. 1)}$$

The imaginary part of the complex refractive index (the extinction index κ) is responsible for the scattering and the absorption of light in the layer and the real part n describes the light refraction. The procedure for deriving τ & ρ of a thick layer or substrate (layers 1, 3, and 5 in Fig. 1) from outside to inside mediums (τ_{oi} and ρ_{oi}) with two standard top and bottom interfaces was explained by Pfrommer [6]. Here standard interface is referred for differentiating from another type of special interface, which will be considered in the next section, consisting on a thin layer structure between two substrate layers, the outer glass and the inner SPD active layer (*layers 2 and 4 in Fig. 1*). The following four steps were considered for determining τ_{oi} and ρ_{oi}. For the moment let consider that outside medium and inside medium are separated by the substrate medium so the assembly consists of air-substrate-air sandwich structure. Two standard interfaces, outside-substrate (o-s) mediums and substrate-inside (s-i) mediums, must be considered. For each top (o-s) and bottom (s-i) interfaces, τ & ρ must be computed:

1st step: Determination of the Fresnel transmission and reflection (t & r) coefficients at normal incidence ($\varphi_o = \varphi_i = 0°$) for S and P polarizations of the two interfaces (o-s and s-i) from refractive index of each medium. Since the optical constants are described using complex refractive index, Fresnel t & r coefficients in Eq. 2 to 5 are observed to be complex numbers, where suffix oi must be considered for top air-substrate and bottom substrate-air interfaces between o-s and s-i mediums respectively:

$$t_{oi}{}^{S} = \frac{2n'_o}{n'_o + n'_i} \qquad \text{(Eq. 2)}$$

$$r_{oi}{}^{S} = \frac{n_o' - n_i'}{n_o' + n_i'} \qquad \text{(Eq. 3)}$$

$$t_{oi}{}^{P} = \frac{2n_o'}{n_o' + n_i'} \qquad \text{(Eq. 4)}$$

$$r_{oi}{}^{P} = \frac{n_i' - n_o'}{n_o' + n_i'} \qquad \text{(Eq. 5)}$$

2nd step: Interface τ & ρ (tau and ro) are computed as the ratio of transmitted and incident power and the ratio of reflected and incident power respectively. The factor of n_i'/n_o' of Eq. 6 and 7 is the reciprocal of the ratio of the media's wave impedances, i.e., the ratio of the transverse components of the electric and magnetic fields at right angles to the direction of propagation and assuming that the magnetic permeability μ is equal to one. The real part of this factor is used in order to avoid complex numbers for interface transmittances [7]. Besides, square absolute values of complex Fresnel t and r coefficients are computed multiplying by their conjugates, where exponent X stands for S or P polarizations. As in the 1st step, suffix oi must be considered for both o-s and i-s interfaces:

$$\tau_{oi}^{X} = Re\left(\frac{n_i'}{n_o'}\right) \cdot \left|t_{oi}^{X}\right|^2 = Re\left(\frac{n_i'}{n_o'}\right) \cdot t_{oi}^{X} \cdot \hat{t}_{oi}^{X} \qquad \text{(Eq. 6)}$$

$$\rho_{oi}^{X} = \left|r_{oi}^{X}\right|^2 = r_{oi}^{X} \cdot \hat{r}_{oi}^{X} \qquad \text{(Eq. 7)}$$

Interface matrix $M_{oi}^{(I)}$ of Eq. 8 using τ_{oi} and ρ_{oi} parameters (i.e., the mean of two S & P polarized τ & ρ) relates I_o^+ & I_o^- and I_i^+ & I_i^-, i.e. the radiation intensity (I) propagating forward (+) and away (-) from an interface in the direction from the outside ("o") to the inside ("i") medium:

$$\begin{bmatrix} I_o^+ \\ I_o^- \end{bmatrix} = \begin{bmatrix} \frac{1}{\tau_{oi}} & \frac{-\rho_{io}}{\tau_{oi}} \\ \frac{\rho_{oi}}{\tau_{oi}} & \tau_{io} - \frac{\rho_{io}\rho_{oi}}{\tau_{oi}} \end{bmatrix} \cdot \begin{bmatrix} I_i^+ \\ I_i^- \end{bmatrix} = M_{oi}^{(I)} \cdot \begin{bmatrix} I_i^+ \\ I_i^- \end{bmatrix} \qquad \text{(Eq. 8)}$$

3rd step: Substrate layer matrix: The extinction (κ) attenuation factor $\Delta_s(d)$ of a thick layer or substrate describing the reduction in intensity of radiation of wavelength λ, from an initially value I_1 to the final value I_2 as it traverses the substrate layer of thickness d, is shown in Equation 9:

$$\Delta_s(d) = \frac{I_2}{I_1} = exp\left(-\frac{4\pi\kappa}{\lambda}d\right) \qquad \text{(Eq. 9)}$$

Substrate layer matrix $N_s^{(I)}$ describing the attenuation of a wave, as it traverses the medium within the substrate layer from initial (1) to final (2) positions, is shown in Equation 10:

$$\begin{bmatrix} I_s^+(1) \\ I_s^-(1) \end{bmatrix} = \begin{bmatrix} \frac{1}{\Delta_s(d)} & 0 \\ 0 & \Delta_s(d) \end{bmatrix} \cdot \begin{bmatrix} I_s^+(2) \\ I_s^-(2) \end{bmatrix} = N_s^{(I)} \cdot \begin{bmatrix} I_s^+(2) \\ I_s^-(2) \end{bmatrix} \qquad \text{(Eq. 10)}$$

4th step: Matrix multiplication: Computing the substrate layer matrix between the two o-s and s-i interface matrices is shown in Equation 11. When illuminating only from the outside medium ("o") in the forward (+) direction, $I_o^+=1$ and $I_i^-=0$. Then, Equation 11 becomes Equation 12 and the forward (+) intensity of the inside medium (I_i^+) and the backward (-) intensity of the outside medium (I_o^-) are related to τ_{oi} and ρ_{oi} respectively, i.e., the τ & ρ of an outside-substrate mediums interface matrix ($M_{os}^{(I)}$), a substrate layer matrix ($N_s^{(I)}$) and a substrate-inside medium interface matrix ($M_{si}^{(I)}$):

$$\begin{bmatrix} I_o^+ \\ I_o^- \end{bmatrix} = M_{os}^{(I)} \cdot N_s^{(I)} \cdot M_{si}^{(I)} \cdot \begin{bmatrix} I_i^+ \\ I_i^- \end{bmatrix} \qquad \text{(Eq. 11)}$$

$$\begin{bmatrix} 1 \\ \rho_{oi} \end{bmatrix} = M_{os}^{(I)} \cdot N_s^{(I)} \cdot M_{si}^{(I)} \cdot \begin{bmatrix} \tau_{oi} \\ 0 \end{bmatrix} \qquad \text{(Eq. 12)}$$

2.3.3 Transmission and reflection (t & r) coefficients of a thin layer or film deposited over a thick layer or substrate

As in previous section for determining τ & ρ of a substrate, two interfaces must be considered for determining τ & ρ of an air-film-substrate-air assembly: outside-film-substrate (o-f-s) medium top special interface and substrate-inside (s-i) mediums standard interface. The only difference with the air-substrate-air assembly of previous section is the substitution of o-s top interface of a substrate by an o-f-s interface of an air-film-substrate top interface. The following three steps were considered for determining the t & r coefficients of a thin film (Toi and Roi, in capital letters to differentiate from the t & r coefficients of a standard interface between two substrates or thick layers):

1st step: Determination of the Fresnel transmission and reflection (t & r) coefficients at normal incidence ($\varphi_o = \varphi_i = 0°$) for S and P polarizations of the two standard interfaces (o-f and f-s), which consist of the top special interface (o-f-s). The t & r coefficients for each interface are derived from refractive index of each mediums using Equations 2 to 5, resulting to be complex numbers, where suffix oi for the top and bottom interfaces are related to outside-film (o-f) and film-substrate mediums (f-s). In case that the top special interface consists of a pile of N thin layers or films, there would be N bottom interfaces. Interface matrix $M_{oi}^{(E)}$ using t & r coefficients is observed in Equation 13 in order to relate E_o^+ & E_o^- and E_i^+ & E_i^-, representing the amplitudes of the net electric fields (E) propagating forward (+) and away (-) from an interface in the direction from the outside ("o") medium to the inside ("i") medium. Here suffix oi must be considered for o-f and f-s first and second interfaces, which are observed in the top special interface for the outside-film-substrate mediums. The bottom standard interface observed is the same substrate-inside mediums interface observed for the previous case of air-substrate-air assembly:

$$\begin{bmatrix} E_o^+ \\ E_o^- \end{bmatrix} = \begin{bmatrix} \frac{1}{t_{oi}} & \frac{r_{oi}}{t_{oi}} \\ \frac{r_{oi}}{t_{oi}} & \frac{1}{t_{oi}} \end{bmatrix} \cdot \begin{bmatrix} E_i^+ \\ E_i^- \end{bmatrix} = M_{oi}^{E} \cdot \begin{bmatrix} E_i^+ \\ E_i^- \end{bmatrix} \qquad \text{(Eq. 13)}$$

2nd step: Film layer matrix: The attenuation factor $\Delta_f(d)$ of a thin layer or film describing the reduction in electric field of radiation of wavelength λ, from an initially value E_1 to the final value E_2 as it traverses the substrate layer of thickness d, is shown in Equation 14:

$$\Delta_f(d) = \frac{E2}{E1} = exp\left(-\frac{2\pi n}{\lambda}d\right) \cdot exp\left(-i\frac{2\pi\kappa}{\lambda}d\right) \qquad \text{(Eq. 14)}$$

Film layer matrix N_f describing the attenuation of a wave, as it traverses the medium within the film layer from initial (1) to final (2) positions, is shown in Equation 15:

$$\begin{bmatrix} E_f^+(1) \\ E_f^-(1) \end{bmatrix} = \begin{bmatrix} \frac{1}{\Delta_f(d)} & 0 \\ 0 & \Delta_f(d) \end{bmatrix} \cdot \begin{bmatrix} E_f^+(2) \\ E_f^-(2) \end{bmatrix} = N_f^{(E)} \cdot \begin{bmatrix} E_f^+(2) \\ E_f^-(2) \end{bmatrix} \qquad \text{(Eq. 15)}$$

3rd step: Matrix multiplication: Computing the film layer matrix between the two o-f and f-s interface matrices is shown

in Equation 16. When illuminating only from the outside medium ("o") in the forward (+) direction, E_o^+=1 and E_i^-=0 and Eq. 16 becomes Eq. 17. The forward (+) net electric field of the inside medium E_i^+ and the backward (-) net electric field of the outside medium E_o^- are related to T_{oi} & R_{oi} respectively (i.e., the t & r coefficients of an outside-film mediums interface matrix $M_{of}^{(E)}$, a film layer matrix $N_f^{(E)}$ and a film-substrate medium interface matrix $M_{fs}^{(E)}$):

$$\begin{bmatrix} E_o^+ \\ E_o^- \end{bmatrix} = M_{of}^{(E)} \cdot N_f^{(E)} \cdot M_{fs}^{(E)} \cdot \begin{bmatrix} E_i^+ \\ E_i^- \end{bmatrix} \qquad \text{(Eq. 16)}$$

$$\begin{bmatrix} 1 \\ R_{oi} \end{bmatrix} = M_{of}^{(E)} \cdot N_f^{(E)} \cdot M_{fs}^{(E)} \cdot \begin{bmatrix} T_{oi} \\ 0 \end{bmatrix} \qquad \text{(Eq. 17)}$$

3. Results and Discussion

3.1 Results

The sandwich structure of Figure 1 considered for the SPD sample consists of two outer glass substrates of 0.5 cm thickness coated on their inner sides with 13-nm-thick ITO films or thin layers, and a centrally positioned 300-µm-thick SPD substrate active layer. In order to calculate the optical constants of the inner SPD active layer, the optical constants of the glass substrates and ITO thin films are required. The complex refractive index of the SPD active layer, numbered "3" in the schematic sandwich structure of Figure 1, is computed by assuming $i_c^{\delta\delta}$=1 and j_c^{00}=0 —i.e., illuminating from the outside air-glass top interface with collimated light and no light incident on the air-glass bottom interface.

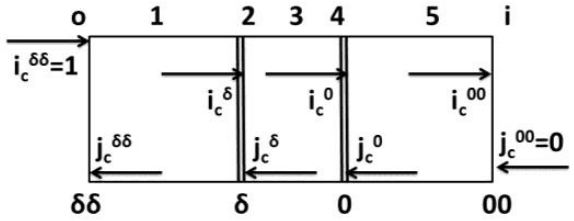

Fig. 1. Sandwich structure of the SPD including two glass substrates (1,5) and two ITO thin films (2,4) surrounding the inner SPD active layer (3).

The results section will be divided in the following parts:

(3.1.1) Glass and Glass/ITO samples

(3.1.2) Outside glass/ITO/SPD/ITO/inside glass sandwich SPD sample

(3.1.3) Intermediate coloration states

(3.1.4) Interface and layers matrices for the SPD sample

3.1.1 Glass and Glass/ITO samples

Two samples, an uncoated glass and a glass covered with ITO, were optically characterized. The complex refractive index of the glass sample (n^G and κ^G) was derived from measurements (T_{dir}^G and R_{spec}^G) by cc eq. of the MLG-4FM, which are appropriate for a thick slab of material. (Fig. 2, [3, 8]). For the ITO-glass sample (measured with that orientation), the Pfrommer model [6] was used with an electric field matrix for the thin layer, which takes into account interference effects. Optical constants of ITO (n^{ITO} & κ^{ITO}) were derived from measurements of T_{dir}^{ITOG} and R_{spec}^{ITOG} once optical constants of glass had been computed from measurements of T_{dir}^G and R_{spec}^G. Complex refractive index of layers 1, 2, 4 and 5 of the sandwich structure diagram of Fig. 1 are then determined and used for determining complex refractive index of inner active SPD layer number 3.

3.1.2 Outside glass/ITO/SPD/ITO/inside glass sandwich SPD sample

Pfrommer model is used to determine the effective optical constants of the inner colored active layer of the SPD sandwich structure, once the optical constants of glass and ITO had been determined, and using a matrix for each layer or interface in the modelled structure. The sandwich structure ("o-1/2/3/4/5-i") presents two outer substrate interfaces of air-glass (o-1) and glass-air (5-i) and two inner interfaces which includes a pair of thin layers (Glass/ITO/SPD (1-3) and SPD/ITO/Glass (3-5)). Layers "2" and "4" correspond to top and bottom ITO thin layers, respectively, and layer "3" stand up the inner SPD active layer. The effective refractive index of the SPD's inner active layer is shown in Fig. 3-a and Fig. 3-*b*.

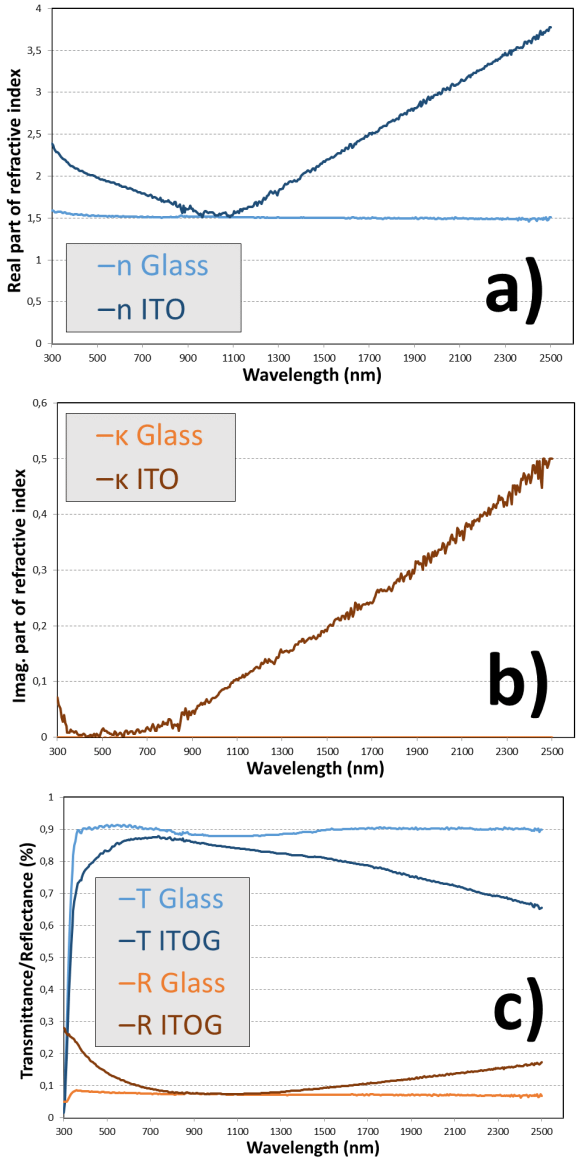

Fig. 2. (a) Real n and (b) imaginary κ parts of the refractive index of Glass and ITO samples. (c) Direct transmittance T_{dir} and specular reflectance R_{spec} of Glass and ITO-Glass samples.

Fig. 3-c and d show measured Tdir and Rspec together with fitted data by Pfrommer model respectively for 0 and 100 Vpeak applied. In this model ITO thin films surrounding

the internal SPD active layer "3" are considered as special interfaces and show absorption. The SPD's real part of the refractive index (Fig. 3-a) shows spurious oscillations coming from similar features in the measurements of Rspec (Fig. 3-d) at the clear "on" state. The real refractive index is slightly higher than the value expected for herapathite (around 1.6 [9]) and a polymer matrix. However, the measurements were carried out on a commercial sample, which may not be completely specified by the structure in Fig.1. For the imaginary part of the refractive index, as expected, the SPD's extinction coefficient is higher for the dark "off" state than for the clear "on" state in the visible wavelength range (Fig.3-b). Herapathite, which is similar to the particle material of the SPD's active layer, is an artificial polyiodide crystal showing extraordinary dichroism so that light rays with different polarizations are absorbed to different amounts [9].

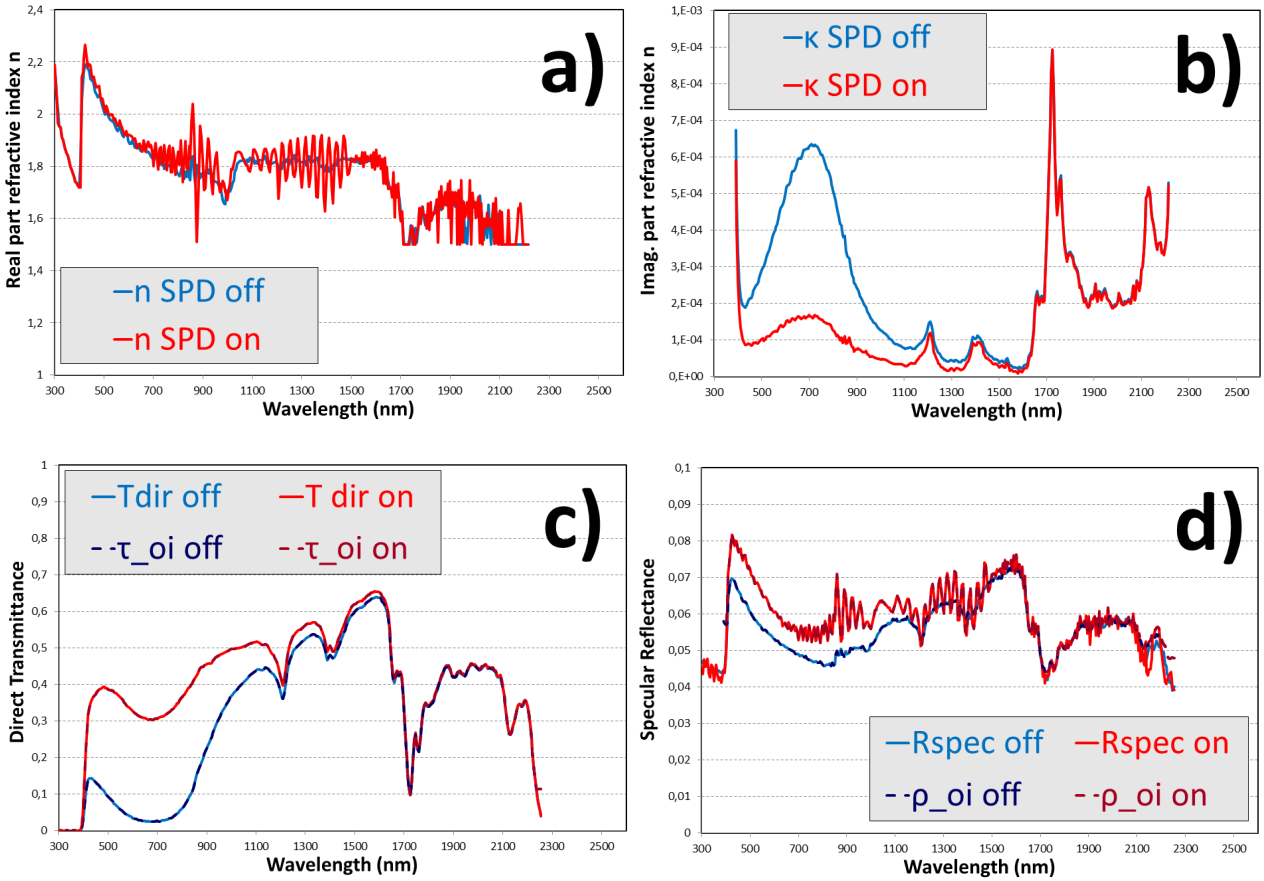

Fig. 3. Spectral values for optical parameters of the SPD sample at clear on states and dark off states, with 100 V_{peak} and 0 applied voltage respectively. (a) real part of the refractive index nSPD (b) imaginary part of the refractive index κ^{SPD}. (c) direct transmittance T_{dir} and τ_{oi} fitting (d) specular reflectance R_{spec} and fitting ρ_{oi}.

3.1.3 Intermediate coloration states

Assuming that the different orientations of dispersed particles for each voltage level cause the different spectral intermediate values of T, intermediate values of R should be related to intermediate values of T and therefore can be estimated. Equation 18 is proposed for estimating intermediate values of R_{tot} and R_{diff}, and hence R_{spec}, from intermediate values of T_{tot} and T_{diff}, being xx from 10 to 90 V_{peak} applied:

$$R_{xx} = R_0 + \frac{T_{xx} - T_0}{T_{100} - T_0} \qquad \text{(Eq. 18)}$$

Due to interferences observed at high wavelength ranges ρ measurements (Fig. 3-d) for the clearest state of the SPD sample with the highest level of applied voltages, for the following figures which reflectances ρ were interpolated computed following Equation 18, the range of following parameters will be cut to 1800 nm instead of at 2500 nm.

3.1.4 Interface and layers matrices for the SPD sample

The transfer of radiation through both coherent (short optical path) and incoherent (thick optical path) layers was considered to compute the net reflectance ρ (ro) and transmittance τ (tau) due to all of the thin and thick layers of the combination observed in the schematic sandwich structure of Fig. 1. Therefore, the procedure of determining interface and layer matrices carried out for the SPD sample consists of determining all the following matrices for electric fields, in order to compute t & r coefficients, and matrices of light intensities, in order to compute tau(τ) and ro (ρ), i.e., the transmittance and reflectance of the shunt of interfaces and layers:

- **$M_{o1}^{(E)}$:** Electric fields (E) interface matrix (M) of Eq. 13 between outside air layer o and top glass substrate layer 1 from t & r coefficients of the top standard interface at both senses of light, i.e., t_{o1} & r_{o1} and t_{1o} & r_{1o}.
- **$M_{o1}^{(I)}$:** Intensities (I) interface matrix (M) of Eq. 8 between outside air "o" layer and top glass substrate

"1" layer from τ & ρ of the top standard interface at both senses of light, i.e., tau_{o1} & ro_{o1} and tau_{1o} & ro_{1o}.

- **$N_1^{(I)}$:** layer matrix (N) which stand for attenuation factor describing the reduction of intensity of the radiation as it traverses the top glass substrate layer 1.
- **$M_{12}^{(E)}$:** Electric field (E) interface matrix (M) of Equation 13 between top glass substrate layer 1 and top ITO thin film layer 2 from t & r coefficients of the top special interface at both senses of light, i.e., t_{12} & r_{12} and t_{21} & r_{21}.
- **$N_2^{(E)}$:** layer matrix (N) which stand for attenuation factor describing the reduction of the electric field of the radiation as it propagates through the 2nd and 3rd interfaces through top ITO film thin layer 2.
- **$M_{23}^{(E)}$:** Electric field (E) interface matrix (M) of Equation 13 between top ITO thin film 2 and the inner active SPD layer 3 from t & r coefficients of the top special interface at both senses of light, i.e., t_{23} & r_{23} and t_{32} & r_{32}.
- **$M_{12}^{(E)}$·$N_2^{(E)}$·$M_{23}^{(E)}$** multiplication matrix Equation 16 solved for t & r coefficients at both senses of light, i.e., T_{13} & R_{13} and T_{31} & R_{31} (capital letters standing for the top thin film ITO layer treated as a special interface showing absorption).
- **$M_{13}^{(I)}$:** Intensities (I) interface matrix (M) of Equation 8 between top glass substrate layer 1 and SPD inner active layer 3 from τ & ρ of the top special interface in both senses of light, i.e., tau_{13} & ro_{13} and tau_{31} & ro_{31}.
- **$N_3^{(I)}$:** SPD inner active substrate layer matrix (N) which stand for attenuation factor describing the reduction of intensity of the radiation as it traverses the inner active SPD substrate layer 3.
- **$M_{o1}^{(I)}$·$N_1^{(I)}$·$M_{13}^{(I)}$** multiplication matrix Equation 12 solved for τ & ρ at both senses of light, i.e., tau_{o3} & ro_{o3} and tau_{3o} & ro_{3o}.
- **$M_{34}^{(E)}$:** Electric fields (E) interface matrix (M) of Equation 13 between SPD inner active layer 3 and bottom ITO film thin layer 4 from t & r coefficients of the top standard interface at both senses of light, i.e., t_{34} & r_{34} and t_{43} & r_{43}.
- **$N_4^{(E)}$:** layer matrix (N) which stand for attenuation factor describing the reduction of the electric field of the radiation as it propagates through the 3rd and 4th interfaces through bottom ITO film thin layer 4.
- **$M_{45}^{(E)}$:** Electric fields (E) interface matrix (M) of Equation 13 between bottom ITO film thin layer 4 and bottom glass substrate layer 5 from t & r coefficients of the top standard interface at both senses of light, i.e., t_{45} & r_{45} and t_{54} & r_{54}.
- **$M_{34}^{(E)}$·$N_4^{(E)}$·$M_{45}^{(E)}$** multiplication matrix Equation 16 solved for t & r coefficients at both senses of light, i.e., T_{35} & R_{35} and T_{53} & R_{53} (capital letters standing for the bottom thin film ITO layer treated as a special interface showing absorption).
- **$M_{35}^{(I)}$:** Intensities (I) interface matrix (M) of Equation 8 between SPD inner active layer 3 and bottom glass substrate layer 5 from τ & ρ of the bottom special interface in both senses of light, i.e., tau_{35} & ro_{35} and tau_{53} & ro_{53}.
- **$N_5^{(I)}$:** layer matrix (N) which stand for attenuation factor describing the reduction of intensity of the radiation as it traverses the bottom glass substrate layer 5.
- **$M_{5i}^{(E)}$:** Electric fields (E) interface matrix (M) of Equation 13 between bottom glass substrate layer 5 and inside air layer "i" from t & r coefficients of the top standard interface at both senses of light, i.e., t_{5i} & r_{5i} and t_{i5} & r_{i5}.
- **$M_{5i}^{(I)}$:** Intensities (I) interface matrix (M) of Equation 8 between bottom glass substrate layer 5 and inside air layer "i" from τ & ρ of the bottom standard interface at both senses of light, i.e., tau_{5i} & ro_{5i} and tau_{i5} & ro_{i5}.
- **$M_{35}^{(I)}$·$N_5^{(I)}$·$M_{5i}^{(I)}$** multiplication matrix Equation 12 solved for τ & ρ at both senses of light, i.e., tau_{35} & ro_{35} and tau_{53} & ro_{53}.
- **$M_{o3}^{(I)}$·$N_3^{(I)}$·$M_{3i}^{(I)}$** multiplication matrix Eq. 12 solved for τ & ρ at both senses of light, i.e., tau_{oi} & ro_{oi} and tau_{io} & ro_{io}.

3.2 Discussion

The treatment of the output data for each level of voltage applied to the SPD sample for the achieved simulated parameters can add more information about the voltage dependence using contour-plots. Two types of contour-plots are considered: spectral voltage contour-plots (SVCP), for each parameter at each voltage level, and spectral voltage-steps contrast contour-plots (SVSCCP), for each parameter at each difference of voltage level between adjacent voltage levels. This section will be divided in the following parts:

(3.2.1) Spectral voltage contour-plots (SVCP)

(3.2.2) Transmittance and reflectance of the inner SPD layer substrate surrounded by ITO thin layer based top and bottom special interfaces (τ_{15} & ρ_{15})

(3.2.3) Transmittance and reflectance of the thin layer ITO film based top and bottom special interfaces (τ_{13}=τ_{53} & ρ_{13}=ρ_{53} and τ_{31}=τ_{35} & ρ_{31}=ρ_{35})

(3.2.4) Spectral voltage-steps contrast contour-plots (SVSCCP)

3.2.1 Spectral voltage contour-plots (SVCP)

τ & ρ voltage dependence of each interface of the setup of layers of the sandwich structure of the SPD sample in Fig. 1 shows different behavior for outer interfaces (between air and glass layers) than for the inner special interfaces showing absorption (between glass, ITO and inner SPD active layer). For outer interfaces (o1 and 5i), the applied voltage level does not affect to the interface τ & ρ since the only change caused by voltage is related to inner SPD active layer number 3. Hence outer interface τ & ρ are voltage independent and do not get affected by the optical appearance of the SPD sample. Besides, they are bidirectional, i.e., they are the same from outside to inside mediums than from inside to outside mediums (τ_{oi}=τ_{io} and ρ_{oi}=ρ_{io}). Concerning inner special interfaces showing absorption, the top inner interface "13" is between top glass substrate layer "1", the top thin film ITO layer "2" and the inner SPD active layer "3". The bottom inner special interface "35" is between the inner SPD active layer "3", the bottom thin film ITO layer "4" and the bottom glass substrate layer "5".

Figures 4 and 5 show the real (n^{SPD}) and imaginary (κ^{SPD}) parts of the refractive index of the inner SPD active layer 3 respectively. Interferences observed in n^{SPD} for high levels of applied voltage (and hence for the clearest optical states of

the SPD) in Fig. 4a cause the differences observed at the SVCP of Fig. 4b. The oscillations for n^{SPD} parameter are observed for cases when $k_2 << n_2$ and a method Swanepoel [10] can be applied in order to retrieve a n^{SPD} parameter without such oscillations, since the real part of the refractive index is related to the speed of light in the medium and should not oscillate in such a high way for adjacent wavelengths.

For κ^{SPD}, the SVCP of Figure 5a shows a vertical uniformity at wavelength ranges where this parameter is independent of the applied voltage, such as for wavelength above 1000 nm, where there are no differences from dark and clear optical appearances of the SPD, with 0 and 100 V_{peak} applied (Fig. 5a). Hence, it could be said that n^{SPD} and κ^{SPD} parameters show a behavior quasi-independent (almost vertical uniformity at the SVCP, Fig. 4b) and dependent (no vertical uniformity at all, Fig. 5b) of the applied voltage, respectively. Since the Swanepoel method would eliminate the oscillations of the quasi-independent behavior of n^{SPD} parameter with the applied voltage, leading to an independent behavior such as outer air-glass τ & ρ parameters at interfaces o1 and 5i. However, this method is not carried out in the present work and will be considered for future works.

Figures 6 and 7 show spectral and SVCP of T_{dir} and R_{spec} respectively. Again, vertical uniformity of contour-plots at some wavelength ranges stands for no change in the parameters for dark and clear states of the SPD sample. This effect is mostly observed at wavelength ranges above 1400 nm. Oscillations of R_{spec} at the clearest optical appearances of the SPD sample for highest voltage levels are due to constructive interferences caused by high transmission of light. These constructive and destructive interferences are not considered in the Pfrommer model and will be studied in future works using Swanepoel method [10]. This interference behavior has also been observed for the clear on states of other smart windows devices based on PDLC [11].

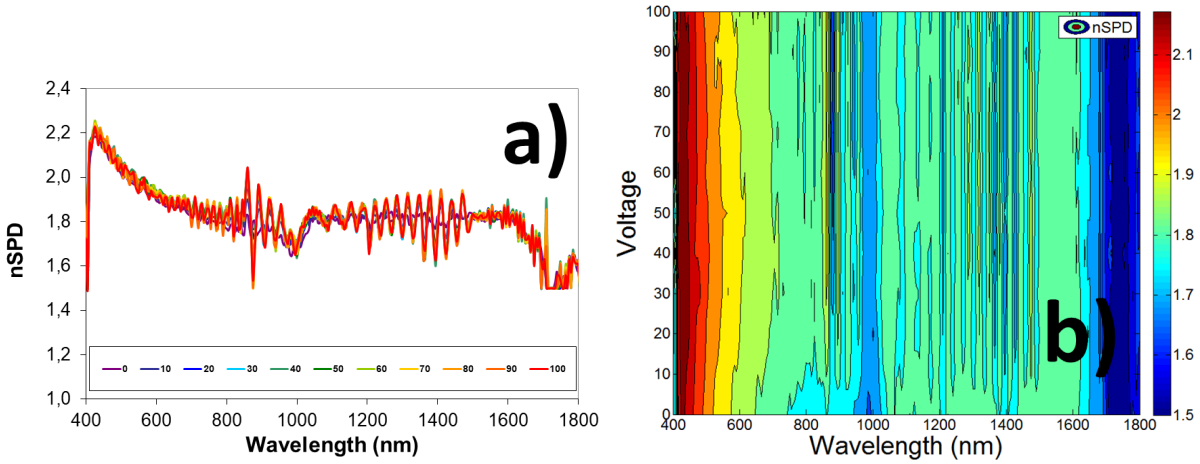

Fig. 4. (a) Spectral real part of the refractive index n^{SPD} for ten levels of voltage, from 0 to 100 V_{peak}. (b) Spectral voltage contour-plot for T_{dir}.

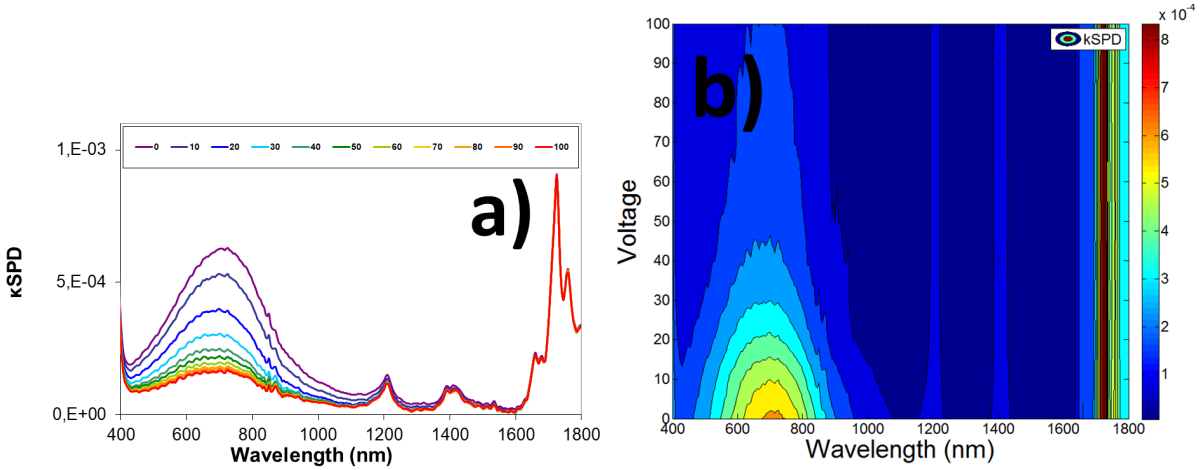

Fig. 5. (a) Spectral imaginary part of the refractive index κ^{SPD} for ten levels of voltage, from 0 to 100 V_{peak}. (b) Spectral voltage contour-plot for T_{dir}.

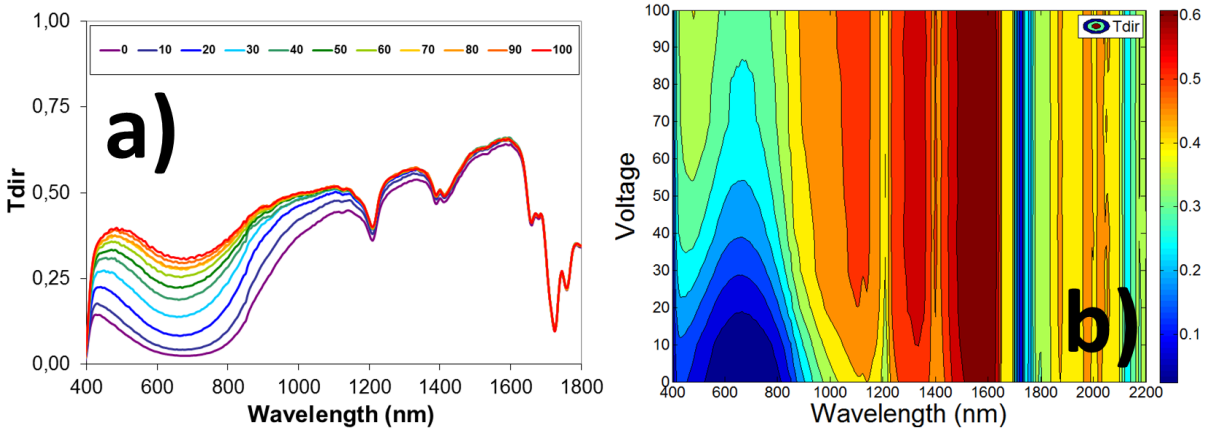

Fig. 6. (a) Spectral direct transmittance T_{dir} from outside air (layer "o") to inside air (layer "i") of Fig. 1 for ten levels of voltage, from 0 to 100 V_{peak}. (b) Spectral voltage contour-plot for T_{dir}.

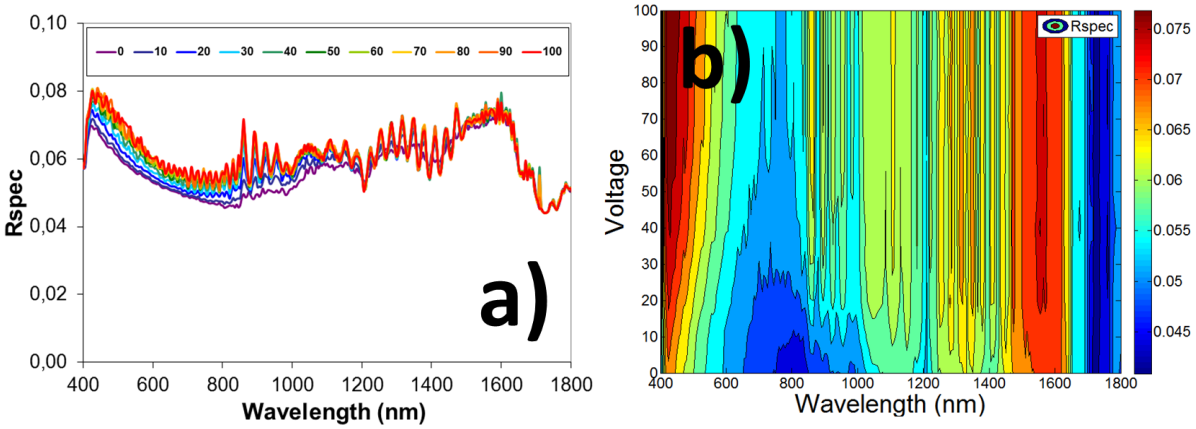

Fig. 7. (a) Spectral specular reflectance R_{spec} from outside air (layer "o") to inside air (layer "i") of Fig. 1, for ten levels of voltage, from 0 to 100 V_{peak}. (b) Spectral voltage contour-plot for R_{spec}.

3.2.2 Transmittance and reflectance of the inner SPD layer substrate surrounded by ITO thin layer based top and bottom special interfaces (τ15 & ρ15)

Figures 8 and 9 show spectral and SVCP of tau_{15} and ro_{15} (τ_{15} & ρ_{15}) parameters, i.e., the τ & ρ of inner layers assembly, consisting on the special interfaces 1-3 and 3-5 (corresponding to the ITO thin layers 2 and 4 respectively) and the inner SPD active layer 3. Here, the outer air-glass (o1) and glass-air (5i) interfaces, together with glass substrate top and bottom layers 1 and 5, were neglected. Equations 19 and 20 are derived from the matrix Pfrommer model [6] to compute τ_{15} & ρ_{15} parameters:

$$\tau_{15} = \frac{\tau_{13} \cdot \tau_{35} \cdot \Delta_3(d)}{1 - \rho_{31} \cdot \rho_{35} \cdot [\Delta_3(d)]^2} \qquad \text{(Eq. 19)}$$

$$\rho_{15} = \rho_{13} + \frac{\tau_{13} \cdot \tau_{31} \cdot \rho_{35} \cdot [\Delta_3(d)]^2}{1 - \rho_{31} \cdot \rho_{35} \cdot [\Delta_3(d)]^2} \qquad \text{(Eq. 20)}$$

Being $\Delta_3(d)$ the substrate attenuation factor of the SPD inner active layer 3 (Equation 9).

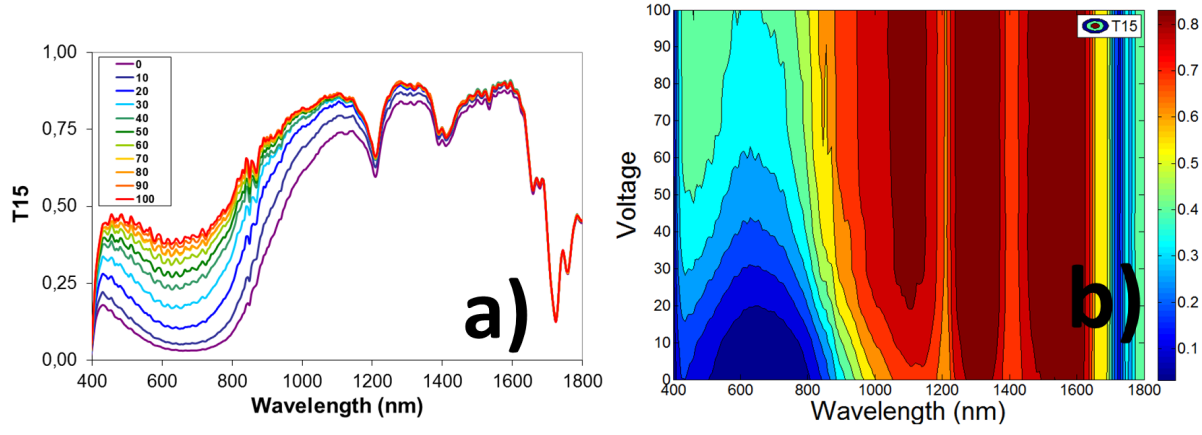

Fig. 8. (a) Spectral direct transmittance tau_{15} from top glass substrate (layer "1") to bottom glass substrate (layer "5") of Fig.1 for ten levels of voltage, from 0 to 100 V_{peak}. (b) Spectral voltage contour-plot for tau_{15}.

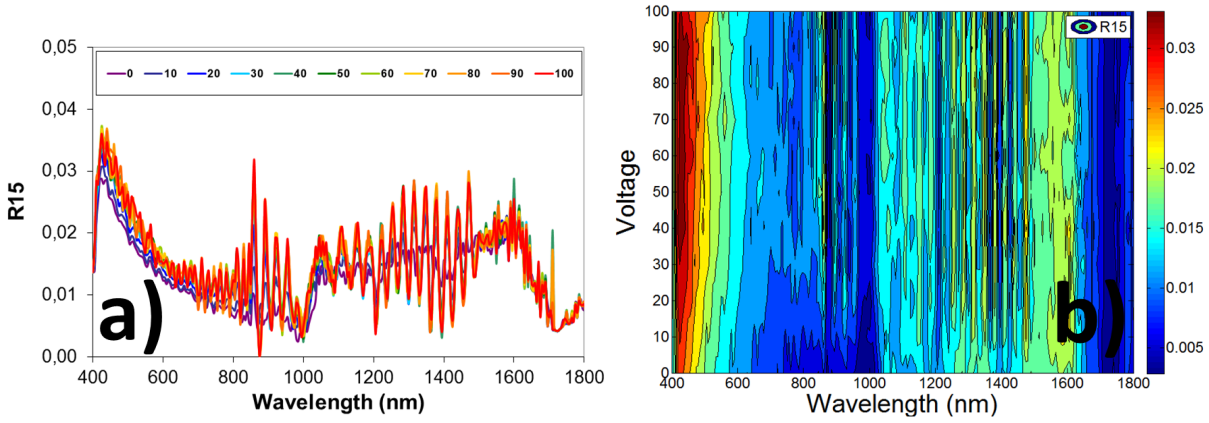

Fig. 9. (a) Spectral specular reflectance ro_{15} from top glass substrate (layer "1") to bottom glass substrate (layer "5") of Fig. 1 for ten levels of voltage, from 0 to 100 V_{peak}. (b) Spectral voltage contour-plot for ro_{15}.

Equations 21 and 22 are used by Kortum [12] for determining τ & ρ of two interfaces (top interface A and bottom interface B) for downwelling and upwelling light beams "i" and "j" respectively:

$$\tau_{AB}^{i} = \frac{\tau_{A}^{i} \cdot \tau_{B}^{i}}{1 - \rho_{A}^{j} \cdot \rho_{B}^{i}} \qquad \text{(Eq. 21)}$$

$$\rho_{AB}^{i} = \rho_{A}^{i} + \frac{\tau_{A}^{i} \cdot \tau_{A}^{j} \cdot \rho_{B}^{i}}{1 - \rho_{A}^{j} \cdot \rho_{B}^{i}} \qquad \text{(Eq. 22)}$$

Comparing Equations 19 & 21 and 20 & 22 it can be deduced the following relations: $\tau_A^i=\tau_{13}$, $\tau_A^j=\tau_{31}\cdot\Delta_s(d)$, $\tau_B^i=\tau_{35}\cdot\Delta_s(d)$, $\rho_A^i=\rho_{13}$, $\rho_A^j=\rho_{31}\cdot\Delta_s(d)$ and $\rho_B^i=\rho_{35}\cdot\Delta_s(d)$. The extinction attenuation factor $\Delta_s(d)$ appears multiplying to τ & ρ parameters of both (top and bottom) special ITO thin layers 2 and 4 only when light crosses the extinction inner SPD active layer 3. For the cases where downwelling light beam "i" crosses the bottom interface B (τ_B^i and ρ_B^i) and for the cases where upwelling light beam "j" crosses top interface A (τ_A^j and ρ_A^j).

Figures 10 and 11 show the spectral and SVCP of parameters τ_{o1} (tau_{o1}) and ρ_{o1} (ro_{o1}). Note that the outer τ & ρ are bidirectional and symmetrical (due to the sandwich structure of the SPD sample), i.e., $\tau_{o1}=\tau_{1o}=\tau_{5i}=\tau_{i5}$ and $\rho_{o1}=\rho_{1o}=\rho_{5i}=\rho_{i5}$. Since the outer τ & ρ parameters are not affected by the optical appearance of the SPD inner active layer 3 (dark or clear), they are independent of the applied voltage and the SVCP result perfectly verticals.

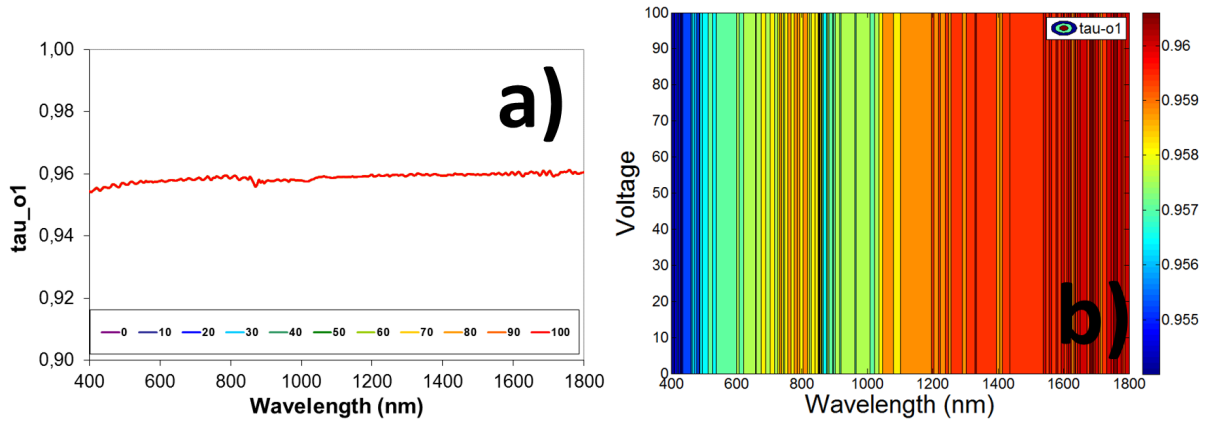

Fig. 10. (a) Spectral direct transmittance tau_{o1} from outside air (layer "o") to top glass substrate (layer "1") of Fig. 1 for ten levels of voltage, from 0 to 100 V_{peak}. (b) Spectral voltage contour-plot for tau_{o1}.

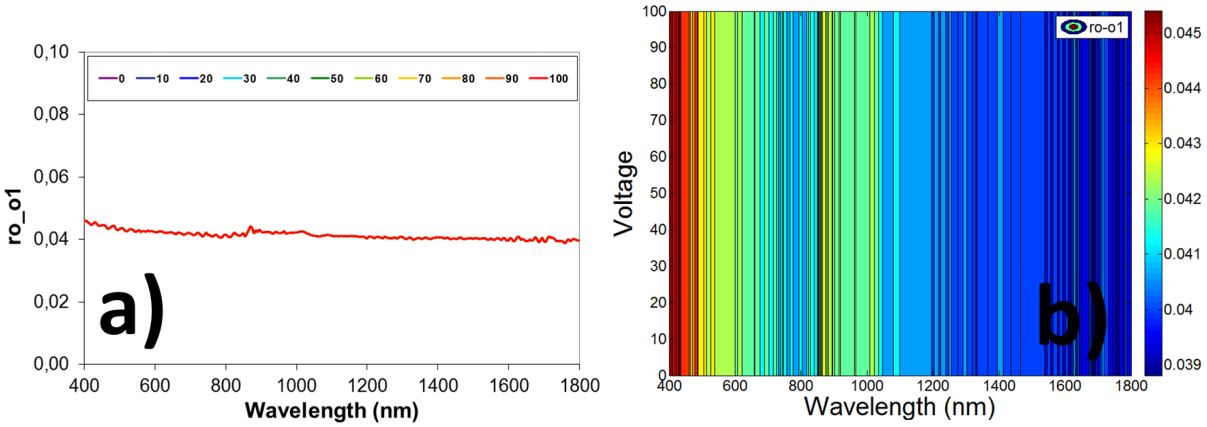

Fig. 11. (a) Spectral specular reflectance ro_{o1} from outside air (layer "o") to top glass substrate (layer "1") of Fig. 1 for ten levels of voltage, from 0 to 100 V_{peak}. (b) Spectral voltage contour-plot for ro_{o1}.

3.2.3 Transmittance and reflectance of the thin layer ITO film based top and bottom special interfaces (τ13=τ53 & ρ13=ρ53 and τ31=τ35 & ρ31=ρ35)

Fig. 12 and 13 show the spectral and SVCP of parameters tau_{13} and ro_{13}, i.e., the τ & ρ of the special top ITO thin layer 2. Their reverse parameters tau_{31} and ro_{31} spectral and SVCP are shown in Fig. 14 and 15. Note the similarity between tau_{13} and tau_{31}, i.e., the transmittance τ of the top ITO thin layer 2 is bidirectional. However, this is not the case for ro_{13} and ro_{31}. Besides, due to the symmetrical sandwich structure (Fig. 1), the spectral and SVCP of parameters for the bottom ITO thin layer 4 are $\tau_{53}=\tau_{13}=\tau_{31}=\tau_{35}$ and $\rho_{53}=\rho_{13}\neq\rho_{31}=\rho_{35}$. Hence, tau_{35} and tau_{53} are bidirectional but not ro_{35} and ro_{53} (and the same substituting 35 with 31 and 53 with 13). The transmittance of a special thin layer is the same no matter the direction considered from outside to inside or vice versa. For reflectance, this is not true. That is why only reflectance for glass-ITO-SPD correspond to 13 and 53 special interfaces and the reflectance to SPD-ITO-glass correspond to 31 and 35 special interfaces.

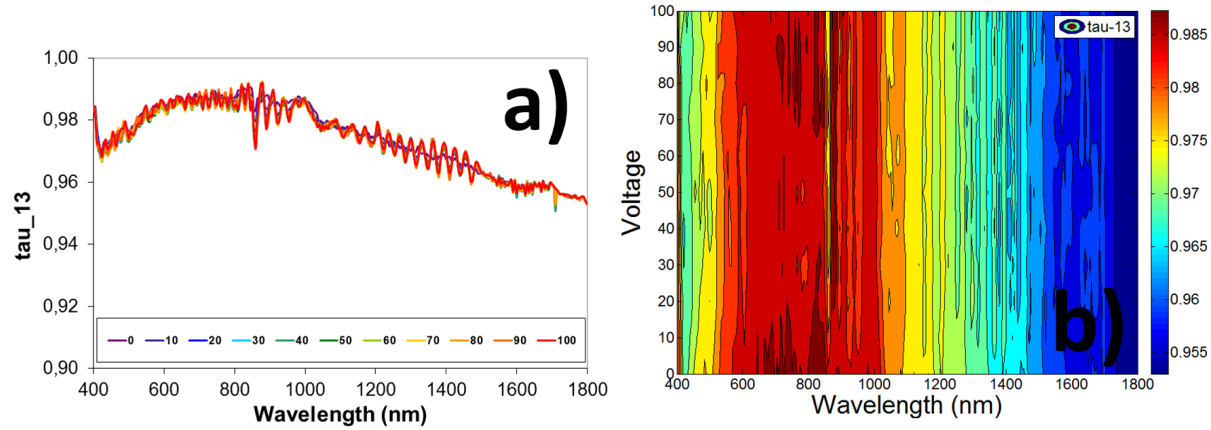

Fig. 12. (a) Spectral direct transmittance tau_{13} from top glass substrate (layer "1") to inner SPD active layer (layer "3") of Fig. 1 for ten levels of voltage, from 0 to 100 V_{peak}. (b) Spectral voltage contour-plot for tau_{13}.

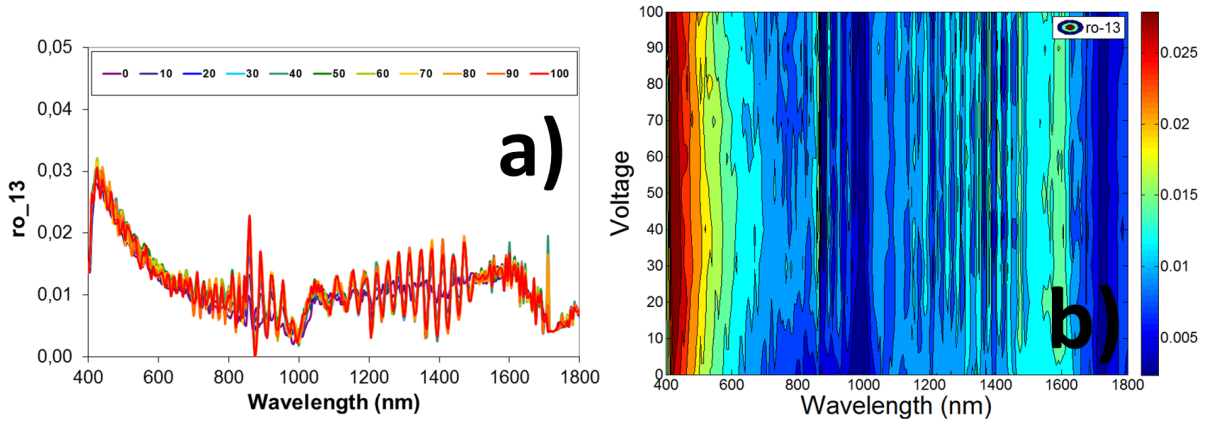

Fig. 13. (a) Spectral specular reflectance ro_{13} from top glass substrate (layer "1") to inner SPD active layer (layer "3") of Fig. 1 for ten levels of voltage, from 0 to 100 V_{peak}.(b) Spectral voltage contour-plot for ro_{13}.

Note that Fig. 12 is the same than Fig. 14 for bidirectional special interface transmittance. However, this is not true for Fig. 13 and Fig. 15 for non-bidirectional special interface reflectance. Special interface transmittance and reflectance are computed using transmission and reflection coefficients retrieved with Equations 13 to 17 used in section 2.3.3 for thin layers structures. Then T_{oi} and R_{oi} parameters of Equation 17 retrieved for oi=13, 31, 35 and 53, i.e., from glass to inner SPD active layer, with the ITO thin layer considered as a special interface showing absorption.

Then, Equations 6 and 7 are used with the T_{oi} and R_{oi} transmission and reflection coefficients of the special interface consisting on a thin film layer separating a glass substrate and SPD inner active substrate layer. These parameters retrieved from Equation 17 were determined in order to compute nSPD and κSPD in Fig. 3. Note also that Swanepoel method [10] can be used as oscillation.

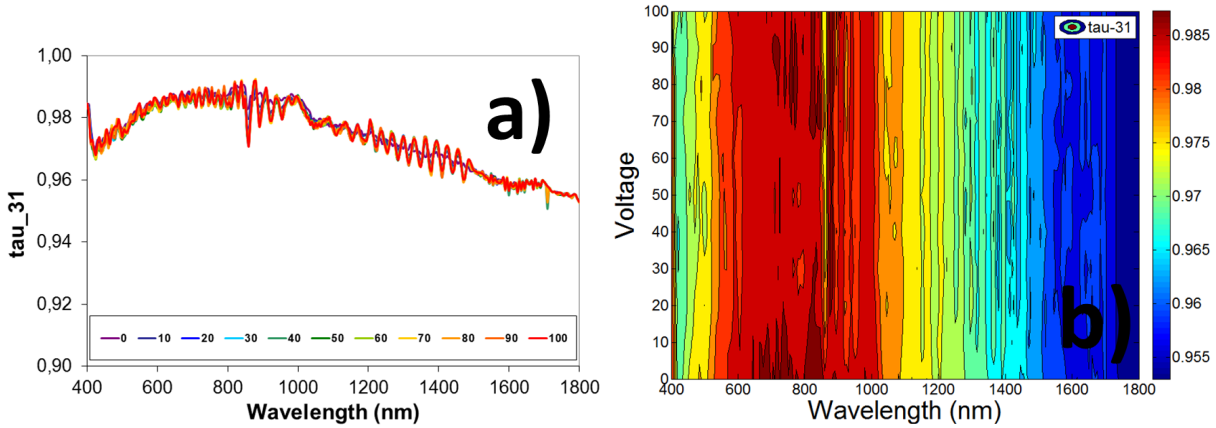

Fig. 14. (a) Spectral direct transmittance tau_{31} from inner SPD active layer (layer "3") to top glass substrate (layer "1") of Fig. 1 for ten levels of voltage, from 0 to 100 V_{peak}. (b) Spectral voltage contour-plot for tau_{31}.

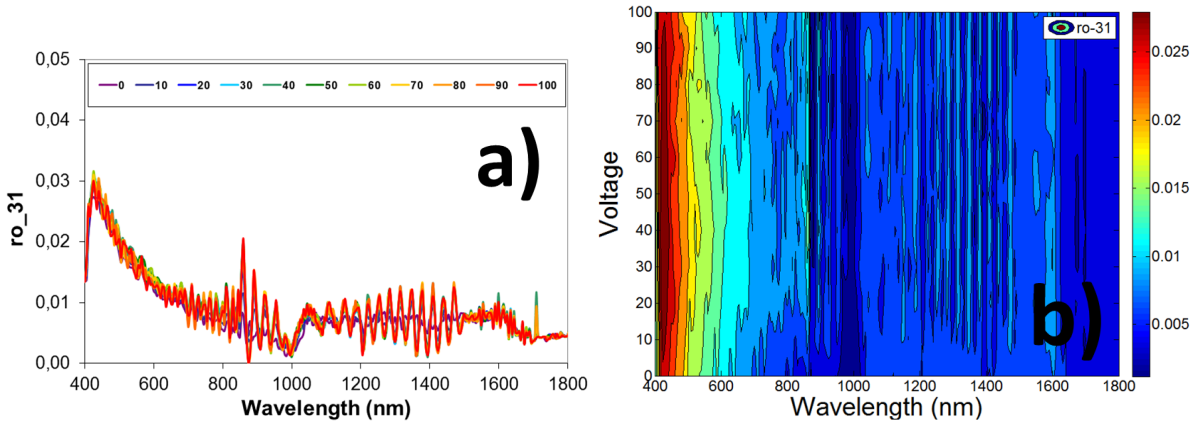

Fig. 15. (a) Spectral specular reflectance ro_{31} from inner SPD active layer (layer "3") to top glass substrate (layer "1") for ten levels of voltage, from 0 to 100 V_{peak}. (b) Spectral voltage contour-plot for ro_{31}.

Using the four relations of Harbecke [18] for t_{oi}, r_{oi}, t_{io} and r_{io} describing the t & r coefficients ($t_{oi}=1/T_{11}$, $r_{oi}=T_{21}/T_{11}$, $t_{io}=T_{11}\cdot T_{22}-T_{12}\cdot T_{21})/T_{11}$ and $r_{oi}=-T_{12}/T_{11}$) for multilayer matrix multiplication, Equations 23 to 24 are derived from Pfrommer matrix model [6] for t & r coefficients of the special interfaces showing absorption. Top and bottom ITO thin layers T_{13} & R_{13} and T_{31} & R_{31} are the same t & r coefficients than T_{53} & R_{53} and T_{35} & R_{35} respectively (in capital letters for differentiating from standard interfaces), which thin layer or film attenuation factor $\Delta_f(d)$ is determined by the of Eq. 14:

$$T_{13} = \frac{1}{T^{11}} = \frac{t_{12}\cdot t_{23}\cdot \Delta_f(d)}{1-r_{21}\cdot r_{23}\cdot \left[\Delta_f(d)\right]^2} \quad \text{(Eq. 23)}$$

$$R_{13} = \frac{T^{21}}{T^{11}} = \frac{r_{12}+r_{23}\cdot \left[\Delta_f(d)\right]^2}{1-r_{21}\cdot r_{23}\cdot \left[\Delta_f(d)\right]^2} \quad \text{(Eq. 24)}$$

$$T_{31} = \frac{T^{11}T^{22}-T^{12}T^{21}}{T^{11}} = \frac{t_{32}\cdot t_{21}\cdot \Delta_f(d)}{1-r_{21}\cdot r_{23}\cdot \left[\Delta_f(d)\right]^2} \quad \text{(Eq. 25)}$$

$$R_{31} = \frac{-T^{12}}{T^{11}} = \frac{r_{32}+r_{21}\cdot \left[\Delta_f(d)\right]^2}{1-r_{21}\cdot r_{23}\cdot \left[\Delta_f(d)\right]^2} \quad \text{(Eq. 26)}$$

Derived Equations 23 to 26 for t & r coefficients are the same than the equations 2-32a, b and 2-33a, b of Knittel [19].

3.2.4 Spectral voltage-steps contrast contour-plots (SVSCCP)

Note that the limits of the vertical axis of this second type of contour-plot, for spectral voltage-steps contrast, are from 10 to 100 V, instead of from 0 to 100 V as in the first type of contour-plot, since SVSCCP show which step of voltage is

more effective for each parameter shown. Hence, the contrast is between adjacent voltage levels and the vertical axis stand for the high level of the step voltage. Checking both up and down plots in Fig. 3 and 16. For instance, the maximum difference of T_{dir} is observed between 10 V and 20 V and between 20 and 30V in the range 700 to 900 nm. At the opposite, real part of refractive index n does not show relevant changes for the different voltage steps. Voltage steps dependence with spectral T_{dir}, R_{spec} and imaginary refractive index k of the inner active layer of the SPD are mainly observed at the visible range. Contour plots showed that, for the first four steps from 0 to 40 V_{peak}, more than 60% of the change of the whole range from 0 to 100 V_{peak} is obtained.

4. Conclusions

The complex refractive index of the SPD's inner active layer at dark and clear states was determined using the Pfrommer matrix model, differentiating between substrates and thin layers. The dependence of each transmittance and reflectance τ & ρ parameter at each interface with the appearance of the SPD sample showed bidirectional behavior and voltage independency of outer standard interfaces, where air and glass substrate layers are involved. However, for inner special interfaces showing absorption, τ & ρ of ITO thin films showed a quasi-independent behavior with the applied voltage used to switch the absorption suspended particles of the SPD sample. Swanepoel method [10] could be applied as future works in order to achieve an independent real part of the refractive index, which show oscillations at the clearest states of the SPD, with low values for extinction. Future works will deal with the determination of intrinsic α^{SPD} & β^{SPD} (MLG-4FM) and the extensive S^{SPD} & K^{SPD} (KM-2FM) scattering and absorption coefficients of four-flux [3] and two-flux [4,5] models, respectively, of the inner SPD active layer by computing the intermediate forward and reverse light beams (Fig. 1) and the diffuse fractions of light at each interface. The study of the t & r coefficients and the collimated τ & ρ will be accompanied with the diffuse τ & ρ for both, the standard outer and the special inner interfaces showing absorption. Diffuse interface reflectance for standard outer interfaces is computed averaging the Fresnel reflection coefficients for the forward hemisphere [20]. Diffuse interface reflectance for special inner interfaces will be studied following Equations 9 and 10 for collimated to diffuse transfers given by Simonot [21]. Besides, a study of the critical angle and the angles of incidence inside of the faces of a clear plate due to light refraction could result into an improvement of the fitting results [22-23]. Previous works of the author with the SPD sample were recently published for monolayer case [24], improving previous works on the monolayer case of the SPD sample [1,2]. Summarizing, the study presented in this work is a continuation of the study carried out in a previous work presented in a relevant international conference [25], which poster is presented at Figure S1 (**Supporting information**). The background coloration of the poster is determined by colorimetry for the direct transmittance from 0 to 100 V AC 50 Hz sinusoidal signal with 10 V steps. As it can be observed, some plots of the present work are included in this previous work, such as Figures 1, 2, 17 and 18. The main contribution of the present work is the study of the voltage dependent optical parameters such as top and bottom special interface transmittances and reflectances inside the SPD sample, concerning those which are related to optical constants of the inner active SPD layer, and the non-voltage dependent optical parameters of those concerning the outer layers of glass substrate and inside or outside air. The same study of optical constants using collimated T&R components for monolayer case [24] was carried out in [27] using polymer dispersed liquid crystals (PDLC) smart windows, which switch between white milky translucent off and transparent on optical states applying 0 and 74 V at 50 Hz AC sinusoidal signal. The simulation of the optical appearance of other types of PDLC smart windows [28] using colorimetry CIE Yxy 1931 space color and sRGB matrix transformation between the chromatic coordinates and the alpha transparency parameter of Macromedia Flash in order to simulate the transparent effect. Same procedure was carried out for colors of Fig. S1 (**Supporting information**) [25].

Supporting Information

Poster presented at the conference of the reference [25].

Acknowledgments

We are grateful to CIDETEC for providing the SPD window, the glass and ITO-Glass samples and to Angstrom Laboratory for carrying out the measurements using the spectrometer based on integrating sphere Perkin Elmer Lambda 900.

Author Contributions

David Barrios contributions: Conceptualization (100%), Data curation (75%), Formal Analysis (75%), Funding acquisition (100%), Investigation (75%), Methodology (75%), Project administration (100%), Resources (100%), Software (75%), Supervision (100%), Validation (100%), Visualization (60%), Writing – original draft (100%), Writing – review & editing (100%). Carlos Alvarez contributions: Data curation (25%), Formal Analysis (25%), Investigation (25%), Methodology (25%), Software (25%), Visualization (40%).

References and Notes

[1] Barrios, D.; Vergaz, R.; Sanchez-Pena, J. M.; Garcia-Camara, B.; Granqvist, C. G.; Niklasson, G. A. *Sol. Energy Mater. Sol. Cells* **2015**, *143*, 613. **[Crossref]**

[2] Barrios, D.; Vergaz, R.; Sanchez-Pena, J. M.; Granqvist, C. G.; Niklasson, G. A. *Sol. Energy Mater. Sol. Cells* **2013**, *111*, 115. **[Crossref]**

[3] Maheu B.; Letoulouzan, J. N.; Gouesbet, G. *Appl. Opt.* **1984**, *23*, 3353. **[Crossref]**

[4] Kubelka, P. *J. Opt. Soc. Am.* **1948**, *38*, 448. **[Crossref]**

[5] Saunderson, J. L. *J. Opt. Soc. Am.* **1942**, *32*, 727. **[Crossref]**

[6] Pfrommer, P.; Lomas, K. J.; Seale, C.; Kupke, C. *Sol. Energy* **1995**, *54*, 287. **[Crossref]**

[7] Orfanidis, S.J. In: Electromagnetic Waves and Antennas. **2016** [Online]. Chapter 5: Reflection and Transmission, eq. 5.3.4. p. 161. Available: **https://www.ece.rutgers.edu/~orfanidi/ewa/**

[8] McPhedran, R. C.; Botten, L.C.; McKenzie, D. R.; Netterfield, R. P. *Appl. Opt.* **1984**, *23*, 1197. **[Crossref]**

[9] West, C. D. *Am. Mineral.* **1937**, *22*, 731. **[Link]**

[10] Swanepoel, R. *J. Phys. E: Sci. Instrum.***1983**, *16*, 1214. **[Crossref]**

[11] Barrios, D. Characterization and Applications of New Electrochromic Devices: Comparison with Other Electrically Controllable Transmittance Technologies. [Doctoral thesis.] Universidad Carlos III de Madrid, Spain, **2012**. **[Link]**

[12] Kortüm, G. Reflectance Spectroscopy: Principles, Methods, Applications, Springer, New York, USA, 1969. **[Crossref]**

[13] Minkov, D. A. *J. Phys. D: Appl. Phys.* **1989**, *22*, 1157. **[Crossref]**

[14] Ruíz-Pérez, J. J.; González-Leal, J. M.; Minkov, D. A.; Márquez, E. *J. Phys. D: Appl. Phys.* **2001**, *34*, 2489. **[Crossref]**

[15] Shaaban, E. R. *J. Phys. Chem. Solids* **2007**, *68*, 400. **[Crossref]**

[16] Shaaban, E. R.; Abdel-Rahman, M.; Dessouky, M. T. *Thin Solid Films* **2007**, *515*, 3810. **[Crossref]**

[17] Shaaban, E. R.; Yahia, I. S.; El-Metwally, E. G. *Acta Physica Polonica-Series A General Physics* **2011**, *121*, 628. **[Crossref]**

[18] Harbecke, B. *Appl. Phys. B:* **1986**, *39*, 165. **[Crossref]**

[19] Knittel, Z. In: Optics of Thin Films John Wiley & Sons Ltd. **1976**.

[20] R. Levinson, R.; Berdahl, P.; Akbari, H. *Sol. Energy Mater. Sol. Cells* **2005**, *89*, 319. **[Crossref]**

[21] Simonot, L.; Hersch, R. D.; Hébert, M.; Mazauric, S. *Appl. Opt.* **2016**, *55*, 27. **[Crossref]**

[22] Kottler, F. *J. Opt. Soc. Am.* **1960**, *50*, 483. **[Crossref]**

[23] Judd, D. B. *Part of Journal of Research of the National Bureau of Standards* **1942**, *29*. **[Crossref]**

[24] Barrios, D.; Alvarez, C.; Miguitama, J.; Gallego, D.; Niklasson, G. A. *Appl. Opt.* **2019**, *58*. **[Crossref]**

[25] Barrios, D.; Alvarez, C.; Niklasson, G. A. Abstract of the XII LIP Laser Light and Interaction with Particles Conference, Texas A&M University, **2018**. **[Link]**

[26] Barrios, D.; Alvarez, C.; Miguitama, J.; Wang, J.; Niklasson, G. A. Abstract of the Proceedings of the Bremen Zoom Workshop on Light Scattering, ed. by Thomas Wriedt, p. 8-11. March **2022**. **[Link]**

[27] Barrios, D.; Alvarez, C.; Miguitama, J. *VI Congreso Internacional CITIS, Universidad Politécnica Salesiana Sede Guayaquil, Ecuador, 2020,* **2020**, *38*, 448. **[Link]**

[28] Barrios, D.; Alvarez, C.; Miguitama, J. *Abstract of the V Congreso Internacional CITIS, Universidad Politécnica Salesiana Sede Guayaquil, Ecuador*, **2019**, *321*. **[Link]**

How to cite this article

Barrios, D.; Alvarez, C. *Orbital: Electron. J. Chem.* **2023**, *15*, 8. DOI: **http://dx.doi.org/10.17807/orbital.v15i1.16470**